

Completing HI observations of galaxies in the Virgo Cluster

G. Gavazzi,¹, A. Boselli,², W. van Driel³, and K. O’Neil⁴,

¹ Universitá degli Studi di Milano-Bicocca, Piazza delle scienze 3, 20126 Milano, Italy
e-mail: giuseppe.gavazzi@mib.infn.it

² Laboratoire d’Astrophysique de Marseille, BP8, Traverse du Siphon, F-13376 Marseille, France
e-mail: alessandro.boselli@oamp.fr

³ Observatoire de Paris, Section de Meudon, GEPI, CNRS UMR 8111 and Université Paris 7, 5 place Jules Janssen, F-92195 Meudon Cedex, France
e-mail: wim.vandriel@obspm.fr

⁴ NRAO, P.O. Box 2, Green Bank, WV 24944, U.S.A.
e-mail: koneil@gb.nrao.edu

12/9/2004

Abstract. High sensitivity (rms noise ~ 0.5 mJy) 21-cm HI line observations were made of 33 galaxies in the Virgo cluster, using the refurbished Arecibo telescope, which resulted in the detection of 12 objects. These data, combined with the measurements available from the literature, provide the first set of HI data that is complete for all 355 late-type (Sa-Im-BCD) galaxies in the Virgo cluster with $m_p \leq 18.0$ mag. The Virgo cluster HI mass function (HIMF) that was derived for this optically selected galaxy sample is in agreement with the HIMF derived for the Virgo cluster from the blind HIJASS HI survey and is inconsistent with the Field HIMF. This indicates that both in this rich cluster and in the general field, neutral hydrogen is primarily associated with late-type galaxies, with marginal contributions from early-type galaxies and isolated HI clouds. The inconsistency between the cluster and the field HIMF derives primarily from the difference in the optical luminosity function of late-type galaxies in the two environments, combined with the HI deficiency that is known to occur in galaxies in rich clusters.

Key words. Galaxies: distances and redshifts – Galaxies: general – Galaxies: ISM – Galaxies: clusters – individual Virgo – Radio lines: galaxies

1. Introduction

Seen from a 25 year perspective, HI observations of galaxies have provided us with some of the most powerful diagnostics of the role of the environment in regulating the evolution of late-type galaxies in the local Universe. This includes the definition of the “HI deficiency” parameter that measures the lack of gas in individual cluster galaxies with respect to their “undisturbed” counterparts in the field (e.g. Haynes & Giovanelli 1984, Solanes et al. 2001 and references therein). It is well established that spiral galaxies in rich clusters which have a normal optical morphology have systematically positive HI deficiency parameters, i.e. a significantly reduced HI content (e.g. Haynes et al. 1984). The pattern of HI deficiency found in spiral galaxies that are members of rich, X-ray luminous clusters was interpreted as due to the dynamical interaction of the galaxy ISM with the hot cluster IGM (e.g. ram-pressure (Gunn & Gott 1972), viscous stripping (Nulsen 1982),

thermal evaporation (Cowie & Songaila 1977) or to the tidal interaction with nearby companions (Merritt 1983) and/or with the cluster potential well (Byrd & Valtonen 1990; Moore et al. 1996)). Since the HI deficiency parameter indicates if a particular galaxy has already passed through the densest cluster region, it is perhaps the most valuable environmental indicator, as it provides a clear signature of a galaxy’s membership of a rich cluster. The Virgo cluster, due to its proximity to us (17 Mpc), has received the most attention in HI studies. Various works (e.g. Chamaraux et al. 1980; Helou et al. 1981; Haynes & Giovanelli 1986; Hoffman et al. 1989, 2003) provided evidence for the presence in the Virgo cluster of a mixture of galaxies with extreme HI deficiencies and galaxies with normal HI contents. This, in conjunction with distance estimates from the Tully-Fisher (1977) relation, provided circumstantial evidence for significant infall onto the Virgo cluster (Tully & Shaya 1984; Gavazzi et al. 1999b, 2002). In addition to these single-dish studies of their global HI properties, the detailed mapping of Virgo cluster galax-

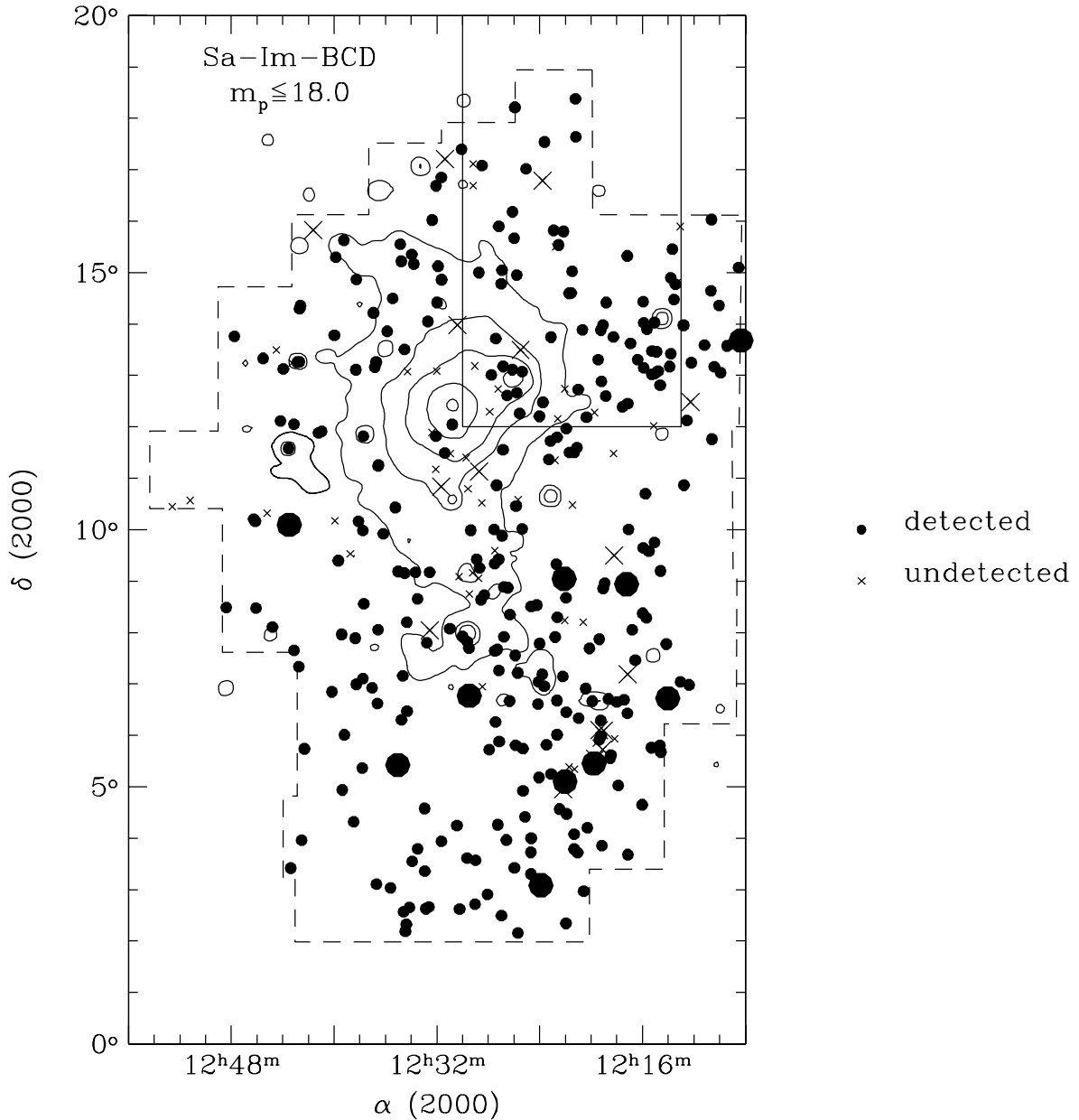


Fig. 1. The Virgo cluster region considered in the present analysis. The dashed broken line represents the boundary of the VCC catalog and the rectangle the area covered by the HIJASS blind HI survey. Superposed are the X-ray contours from ROSAT (Böhringer et al. 1994). All 355 late-type (Sa-Im-BCD) members of the Virgo cluster with $m_p \leq 18.0$ are shown divided into H_I detected (296) and undetected (59). Large symbols refer to objects observed in this work.

ies with radio synthesis telescopes (e.g., Warmels 1986; Cayatte et al. 1990) provided evidence that H_I ablation occurs outside-in, producing a spatial truncation of the H_I disks (Cayatte et al. 1994).

Practically all H_I studies of Virgo galaxies were carried out by pointed observations of individual, optically se-

lected galaxies. Conversely, the first blind H_I survey of a $4^{\circ} \times 8^{\circ}$ area of the Virgo cluster with the 76m Jodrell Bank multibeam instrument (Davies et al. 2004) resulted in the detection of 2 isolated H_I clouds, besides that of 27 previously catalogued galaxies above the survey's H_I mass limit of $5 \times 10^7 M_{\odot}$ for a galaxy with a 50 km s^{-1} linewidth. A

higher sensitivity, full-cluster blind H_I survey of the Virgo cluster is planned for 2005-2006 with the ALFA multibeam system at Arecibo (<http://alfa.naic.edu/>). In preparation for this survey we decided to complete with the present single-beam Arecibo system the pointed observations of late-type (Sa-Im-BCD) galaxies with $m_p \leq 18.0$ mag in the Virgo cluster area. Here we report on the results of these observations which, in conjunction with the previously available H_I data-set, enable us to review the properties of galaxies in this cluster as obtained from optically selected H_I observations.

The selection of the cluster targets for H_I observations is described in Section 2, the observations and the data reduction are presented in Section 3 and the results in Section 4. A discussion of the H_I mass function, as derived from a complete optically selected sample is given in Section 5 and the conclusions are presented in Section 6.

2. Sample selection

All data on the Virgo cluster galaxies are collected and made available worldwide via the "Goldmine" WWW site (<http://Goldmine.mib.infn.it>; see Gavazzi et al. 2003). The H_I completeness of the database is remarkable: the majority ($\sim 80\%$) of disk (Sa-Im-BCD) galaxies with $m_p \leq 18.0$ mag belonging to the Virgo cluster has been detected in H_I and for most of the remaining galaxies significant upper limits are available. The present work is aimed at completing the data on this optically selected sample with high sensitivity (rms ~ 0.5 mJy) H_I observations. Our selection criterion includes all 355 disk (Sa-Im-BCD) galaxies with $m_p \leq 18.0$ mag that are members, i.e. their measured redshift is in the interval $-500 < V < 3000$ km s $^{-1}$, or bona-fide members of the Virgo cluster, i.e. 26 objects without a direct redshift measurement, that have been classified as belonging to the cluster according to the surface brightness criterion used by Binggeli et al. 1985 in the compilation of the Virgo Cluster Catalog (VCC hereafter), and that were subsequently assigned to a particular Virgo sub-cloud by Gavazzi et al. (1999b), using a positional criterion. We include in the target sample all (14) VCC galaxies meeting the above optical selection criterion that were not observed previously in H_I namely: VCC 1, 99, 227, 256, 275, 315, 517, 528, 531, 675, 679, 1237, 1358 and 1597. Moreover we targeted the 19 undetected VCC galaxies that were observed previously with an rms noise level of 0.7 mJy or higher, namely: VCC 48, 222, 323, 341, 358, 362, 524, 666, 802, 1086, 1121, 1189, 1196, 1287, 1377, 1435, 1448, 1885 and 1970.

A map of the Virgo cluster region is shown in Fig. 1 where all (355) galaxies meeting the above selection criterion are shown with the contours of the X-ray emission from the cluster measured by ROSAT (Böhringer et al. 1994) superimposed. Including the measurements obtained for this work, all galaxies have been surveyed in H_I with 296 detections and 59 upper limits.

3. Observations

Using the refurbished 305-m Arecibo Gregorian radio telescope we observed 57 galaxies in the Virgo cluster and Coma supercluster (see Section 2) in February 2004, for a total of 28 hours observing time. Data were taken with the L-Band Wide receiver, using nine-level sampling with two of the 2048 lag subcorrelators set to each polarization channel. All observations were taken using the position-switching technique, with the blank sky (or OFF) observation taken for the same length of time, and over the same portion of the telescope dish as was used for the on-source (ON) observation. Each 5min+5min ON+OFF pair was followed by a 10s ON+OFF observation of a well-calibrated noise diode. The overlaps between both sub-correlators with the same polarization allowed a contiguous velocity search range while ensuring an adequate, wide coverage in velocity. The velocity search range was -1000 to 8500 km s $^{-1}$. The velocity resolution was 2.6 km s $^{-1}$. The instrument's HPBW at 21 cm is $3.5' \times 3.1'$ and the pointing accuracy is about 15''. The pointing positions used are the optical center positions of the target galaxies listed in Table 1. Calibration corrections are good to within 10% (and often much better), see the discussion of the errors involved in O'Neil (2004).

Using standard IDL data reduction software available at Arecibo, corrections were applied for the variations in the gain and system temperature with zenith angle and azimuth. A baseline of order one to three was fitted to the data, excluding those velocity ranges with H_I line emission or radio frequency interference (RFI). The velocities were corrected to the heliocentric system, using the optical convention, and the polarizations were averaged. All data were boxcar smoothed to a velocity resolution of 12.9 km s $^{-1}$ for further analysis. For all spectra the rms noise level was determined and for the detected objects the central line velocity, the line widths at, respectively, the 50% and 20% level of the peak, and the integrated line flux were determined. No flux correction for source to beam size was applied because the optical extent of all detected targets does not significantly exceed the Arecibo beam.

4. Results

In order to identify sources whose H_I detections could have been confused by nearby galaxies, we queried the NED, HyperLeda and Goldmine databases and inspected DSS images over a region of 10' radius surrounding the central position of each source, given the telescope's side-lobe pattern. Quoted values are weighted averages from the HyperLeda database, unless otherwise indicated.

The H_I spectra of both the clearly and the marginally detected galaxies are shown in Figure 2 and the global H_I line parameters are listed in Table 1. These are directly measured values; no corrections have been applied to them for, e.g., instrumental resolution. Table 1 is organized as follows:

Column 1: Obj. is the galaxy designation;

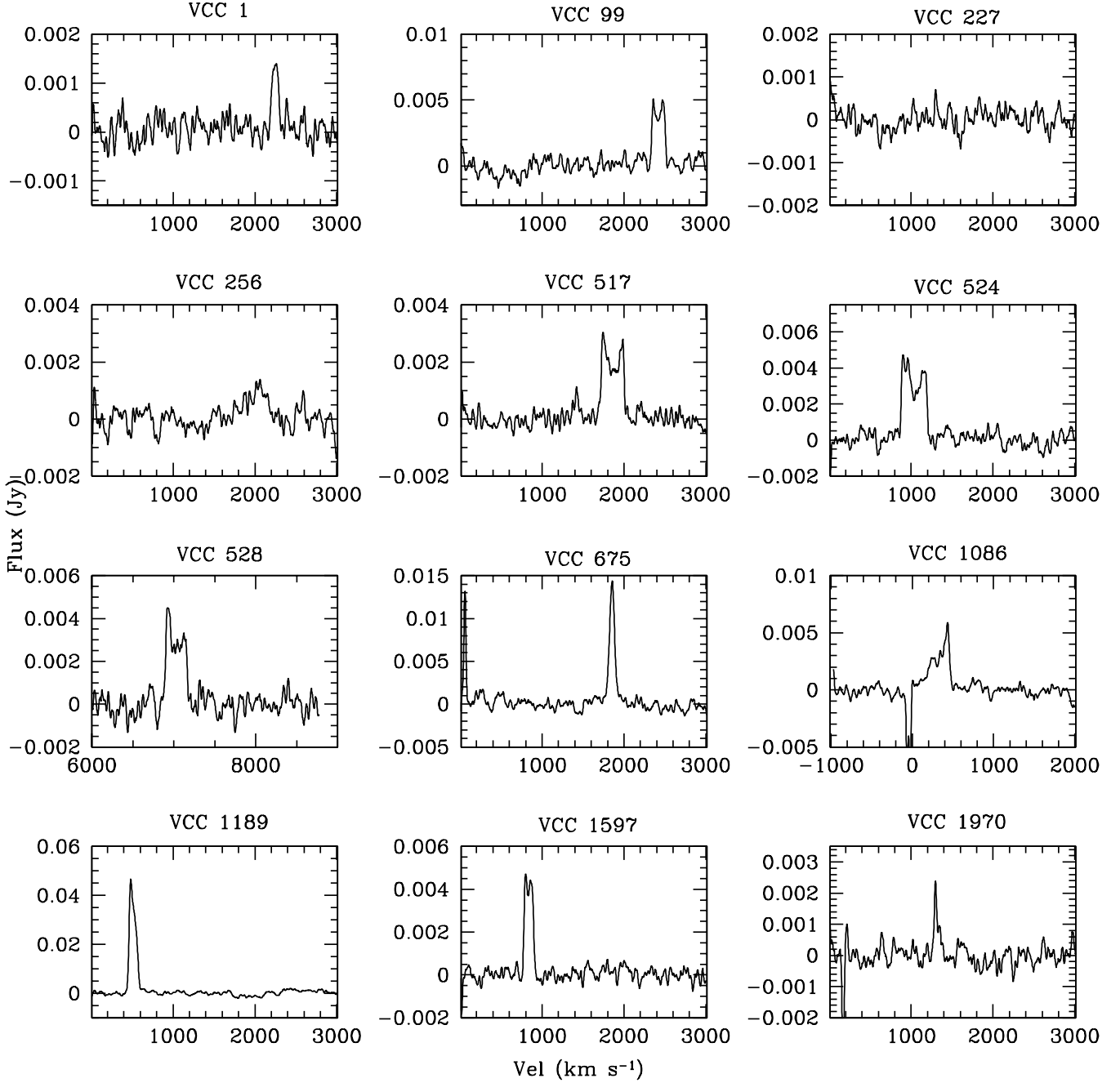


Fig. 2. H_I spectra of the tentatively detected galaxies in the Virgo cluster.

Column 2-3: (J2000) celestial coordinates;
 Column 4: the heliocentric optical recessional velocity (in km s^{-1});
 Column 5: the rms dispersion in the baseline (mJy);
 Column 6: S_p is the peak flux of the detected line (mJy);
 Column 7: V_{HI} is the heliocentric central radial velocity of a line profile (in km s^{-1}), in the optical convention, with its estimated uncertainty (see below);
 Columns 8-9: W_{50} and W_{20} are the line widths at 50% and

20% of peak maximum, respectively, (km s^{-1});
 Column 10: I_{HI} is the integrated line flux (Jy km s^{-1}), with its estimated uncertainty (see below).
 Column 11: A quality flag to the spectra is given, where Q=1 stands for high signal-to-noise, double horned profiles, Q=2 for high signal-to-noise, single horned profiles, and Q=3,4 for low signal-to-noise profiles whose measured line parameters are not reliable.
 We estimated the uncertainties $\sigma_{V_{HI}}$ (km s^{-1}) in V_{HI} and

$\sigma_{I_{HI}}$ (Jy km s⁻¹) in I_{HI} following Schneider et al. (1986, 1990), as:

$$\sigma_{V_{HI}} = 1.5(W_{20} - W_{50})X^{-1} \quad (1)$$

and

$$\sigma_{I_{HI}} = 2(1.2W_{20}/R)^{0.5}R\sigma = 7.9(W_{20})^{0.5}\sigma \quad (2)$$

where I_{HI} is the integrated line flux (Jy km s⁻¹), R is the instrumental resolution (12.9 km s⁻¹), and X is the signal-to-noise ratio of a spectrum, i.e. the ratio of the peak flux density S_p and σ , the rms dispersion in the baseline (Jy). The uncertainty in the W_{20} and W_{50} line widths is expected to be 2 and 3 times $\sigma_{V_{HI}}$, respectively.

Of the 33 observed Virgo cluster objects, 12 (36%) were detected, of which 4 tentatively (see Table 1).

5. Discussion

The newly obtained H_I data were combined with those available from the literature for the $m_p \leq 18.0$ late-type (Sa-Im-BCD)¹ galaxies in the Virgo cluster, listed in Table 2. The sample comprises 355 galaxies, of which 296 were detected and 59 remain undetected.

The compilation of H_I data from the literature was carried out using a criterion of maximum reliability and homogeneity, i.e. recent Arecibo data were preferred to more ancient measurements. In most cases we were able to assess a quality flag to the quoted measurement by inspecting the individual H_I profiles. It is known that the H_I distribution in normal late-type galaxies spatially exceeds the optical extent by a factor ranging from 1.2 (Hewitt et al. 1983) to 2 (Salpeter & Hoffman, 1996) on average. Not accounting for such an effect makes the measurement of the total H_I flux significantly underestimated from single pointing observations of galaxies comparable in size to the beam (see Sullivan et al. 1981, Hewitt et al. 1983). Although this is not a big concern for galaxies observed in this work, because they are generally small compared to the Arecibo beam, it might be a problem for 107/355 galaxies with optical diameters > 2 arcmin, whose H_I parameters have been taken from the literature. In order to minimize the missing flux problem we took the published H_I parameters by selecting the references with the following priority: interferometer or mapping surveys were preferred to single beam pointings. Among the latter works we first selected those which include the flux correction for source to beam size. Only a small fraction of the large galaxies (14/107) were taken from references not including such a correction, that was not either applied by us. The reader should be aware that a possible overestimate of the H_I deficiency parameter among some of the largest (most luminous) galaxies might arise from this effect.

Distances were estimated as in Gavazzi et al. (1999b): individual objects were assigned to the various subclouds in the Virgo cluster according to a positional/velocity

¹ Galaxies of type S..., dE/Im and “?” are not included in the present analysis.

Table 3 Adopted parameters of the M_{HI} vs. diameter relation.

Type	a	b
Sa-Sab	7.17	1.64
Sb	7.29	1.66
Sbc	7.27	1.70
Sc	6.91	1.90
Scd-Im-BCD	7.00	1.88

criterion: A=cluster A (M87), B= cluster B (M49), W=west cloud, M=M cloud, N=North cloud, E=East cloud, S=Southern extension. For each cloud a mean distance D is assumed: 17 Mpc for clouds A, E, S and N, 23 Mpc for cloud B, and 32 Mpc for clouds W and M. We estimate that the distances of individual objects are subject to $\sim 30\%$ uncertainties.

The corrected H_I flux was transformed into H_I mass or mass limit, in solar units, adopting $M_{HI} = 2.36 \cdot 10^5 D^2 I_{HI}$. For undetected galaxies we set $I_{HI} = 1.5 \times \text{rms}_{HI} \times W_{<20-50>}$, where rms_{HI} is the rms of the spectra in mJy and the $W_{<20-50>}$ profile width is based on the following average line widths of the detected objects per Hubble type bin: 300 km s⁻¹ for Sa-Sbc, 190 km s⁻¹ for Sc-Scd, and 85 km s⁻¹ for Sm-BCD;

We also estimate the H_I deficiency parameter following Haynes & Giovanelli (1984) as the logarithmic difference between M_{HI} of a reference sample of isolated galaxies and M_{HI} actually observed in individual objects: $Def_{HI} = LogM_{HI \text{ ref.}} - LogM_{HI \text{ obs.}}$. $LogM_{HI \text{ ref}}$ has been found linearly related to the galaxies linear diameter d as: $LogM_{HI \text{ ref}} = a + b \log(d)$, where a and b are weak functions of the Hubble type, as listed in Table 3. The problem here is that Haynes & Giovanelli (1984) have included in their reference sample of isolated galaxies only relatively large ($a > 1$ arcmin) UGC objects so that the Def_{HI} parameter is poorly calibrated for smaller objects, making determinations of the H_I deficiency for the smallest objects uncertain, likely underestimated (Solanes 1996). Furthermore, as discussed in Solanes et al. (2001) galaxies in the latest Hubble types (Scd-Im-BCD), for which we have adopted a and b parameters consistent with those of Sc (Table 3), are more subject to observational biases than higher surface brightness galaxies. The reader should be aware that the determinations of the H_I deficiency for these objects is highly uncertain.

5.1. Comparison with Leda

The H_I fluxes listed in Table 2 were compared to the H_I fluxes listed in the HyperLeda database (<http://foehn.univ-lyon1.fr/hypercat/>), found for 286 detected galaxies. The comparison of the two datasets is given in Fig. 3, showing excellent agreement: $I_{HI}(T.W.) = I_{HI}(\text{Leda}) * 1.04 \pm 0.25$. The most discrepant objects are VCC 66, 1987 and 2070 for which our flux is almost twice the flux in Leda, and VCC 1673 showing the reverse ratio. Assuming that the two data-sets are independent (which

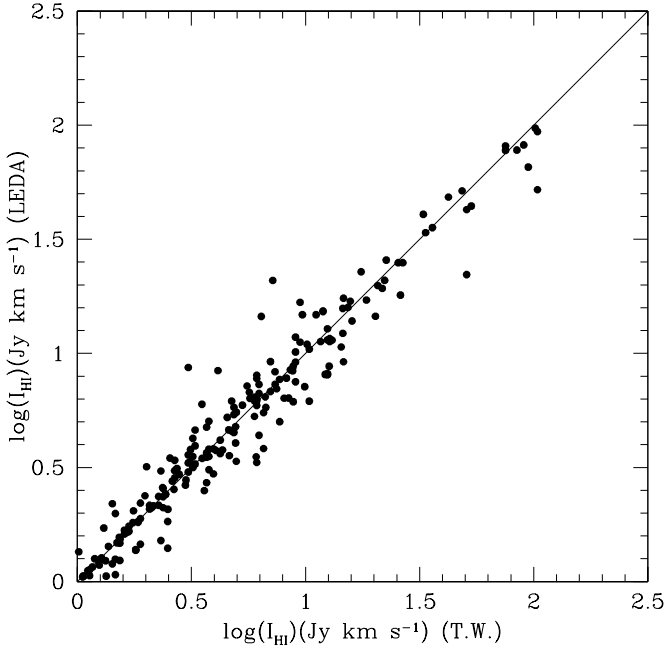


Fig. 3. Comparison of the HI fluxes adopted in this work and those found in the Leda database.

is not true because several measurements are in common) and assuming that the error is equally distributed among the two databases, we estimate that the flux uncertainty given in this work is $\sim 20\%$. Combining this error with the distance uncertainty ($\sim 30\%$) discussed in the previous Section we conclude that the uncertainty on the M_{HI} estimates is $\sim 50\%$, or ~ 0.2 on $\log(M_{HI})$.

5.2. Comparison with HIJASS

It is worth comparing the HI masses listed in Table 2 with those obtained by the HIJASS blind Virgo cluster HI survey (Davies et al. 2004, hereafter D04) for the common galaxies in the area: $12^{\mathrm{h}}13^{\mathrm{m}} < R.A.(J2000) < 12^{\mathrm{h}}30^{\mathrm{m}}$; $+12^{\circ}00' < dec < +20^{\circ}00'$. They are marked as "D04" in the references to Table 2. Out of the 27 galaxies detected by HIJASS only 22 are included in our Table 2 because 3 are not in the VCC and 2 others, which were considered as spirals by HIJASS, are classified as S0 and "?" in the VCC, and were thus not considered by us. The remaining 22 galaxies were detected also in the present survey. Moreover D04 narrowed their search velocity range to $500-2500 \text{ km s}^{-1}$ in order to avoid Galactic emission and background galaxies. Galaxies in common with D04, in the interval $500-2500 \text{ km s}^{-1}$, are marked with an asterisk in Table 2. With these restrictions, the HI mass measured by D04, re-scaled to the distance adopted by us (i.e. 17 Mpc for cluster A, and 32 Mpc for cloud M, instead of 16 Mpc adopted by D04) is plotted vs. our mass estimates in Fig. 4, including galaxies undetected by D04 that are plotted at $M_{HI} = 10^{7.7} \text{ M}_\odot$ (triangles). Two galaxies (VCC 119 = UGC 7249, VCC 483 = NGC 4298) are undetected by D04

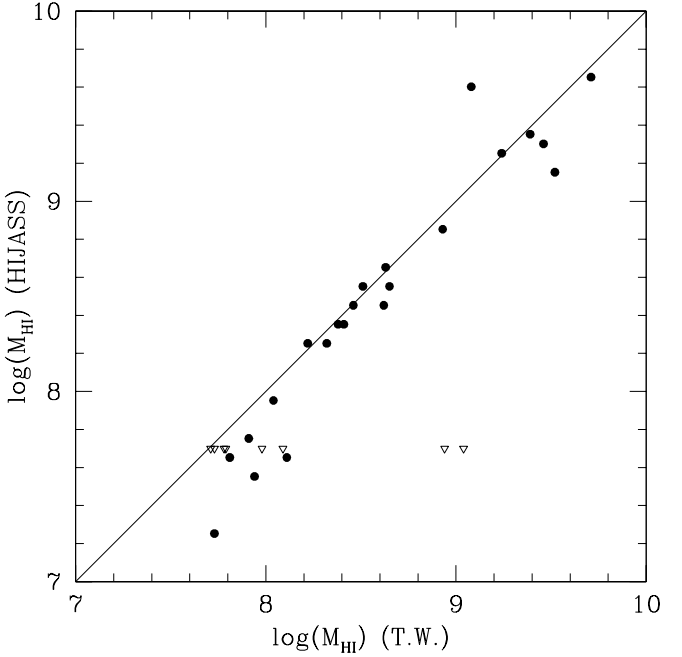


Fig. 4. Comparison of the HI masses as derived from this work with those derived in the blind HIJASS HI survey (Davies et al. 2004) for galaxies in common in the radial velocity interval of $500-2500 \text{ km s}^{-1}$. Open triangles are for undetected HIJASS galaxies.

in spite of their mass in excess of $10^{8.9} \text{ M}_\odot$. However the first has a velocity (622 km s^{-1}) close to the HIJASS limit and NGC 4298 is confused with NGC 4302 (detected in HIJASS with $M_{HI} = 10^{9.2} \text{ M}_\odot$). Altogether the two mass estimates appear consistent with each other, with the exception of a few points at $M_{HI} < 10^8 \text{ M}_\odot$ that appear slightly underestimated by D04.

5.3. The Virgo HI mass function (HIMF)

The data of our optically selected Virgo cluster galaxy sample as listed in Table 2, disregarding the undetected galaxies, were binned in $\log(M_{HI}) = 0.5$ intervals, i.e. ~ 2.5 times the estimated uncertainty on $\log(M_{HI})$ and were used to construct the Virgo HIMF shown in Fig. 5 (solid histogram) and to compare it with the HIJASS HIMF of D04 (filled squares). The latter was normalized to our data by the ratio of the areas covered by the two surveys (a factor of 4.5) and by the ratio (a factor of 1.7) of the number of galaxies in the velocity interval $-500 < V < 3000 \text{ km s}^{-1}$ surveyed by us and those in the interval $500 < V < 2500 \text{ km s}^{-1}$ surveyed by D04. Moreover the HIMF of D04 was shifted toward higher masses by $\log M_{HI} = 0.05$ to account for the slightly larger distances assumed by us (see Sect. 5.2). In addition, Fig. 5 shows the Field HIMF of Zwaan et al. (2003) arbitrarily normalized to our data. In spite of the different construction methods the two Virgo HIMF are surprisingly consis-

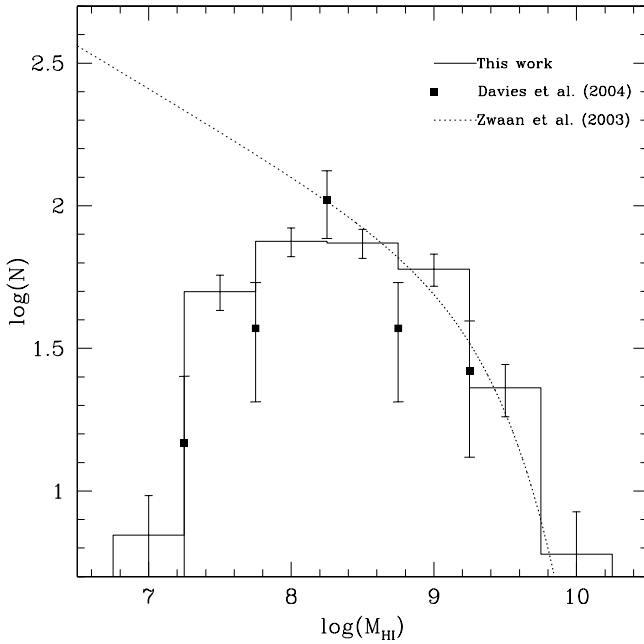


Fig. 5. The Virgo cluster H I mass function (HIMF) as derived from this work using only the detected galaxies (histogram), together with the HIMF derived from the blind HIJASS survey (D04), normalized to our data as described in the text. Error bars represent purely statistical errors. For comparison, the dotted line gives the Field HIMF as derived by Zwaan et al. (2003), normalized arbitrarily in order to match our data at $M_{HI} = 10^{9.5}$ M \odot .

tent with each other². Both HIMFs show a maximum at $M_{HI} \sim 10^{8.5}$ M \odot and a consistent negative slope for lower masses. Below $M_{HI} \sim 10^{8.5}$ M \odot the two are inconsistent with the field HIMF which follows the slope +1.3. The consistency between the Virgo radio- and optically-selected HIMFs in Fig. 5 is not obvious. It implies that the contribution from isolated H I clouds is negligible. Extrapolating from the 2 confirmed detections of D04 to the 7.5 times larger area covered in the present survey, only 15 such objects are expected in the whole cluster (that are missed by an optically selected H I survey). It also implies that, besides the isolated H I clouds, the bulk of the H I emission is associated with the late-type galaxies, with a negligible contribution from the early-type objects that we did not survey in H I³. We show in Fig. 6 that also for the field the observed HIMF can be obtained purely from the contribution of the late-type population. Using the relation $\log M_{HI} = 2.9 - 0.34 \times M_p$, which holds on average between the H I mass and the optical lu-

² The point at $M_{HI} = 10^{8.25}$ M \odot of D04 includes 14 detections, 2 of which correspond to isolated H I clouds – disregarding these two objects the discrepancy with the optical selected HIMF becomes negligible.

³ A dozen H I detections were reported in Virgo associated with early-type galaxies. These have not however been surveyed with completeness. None belongs to the D04 sample.

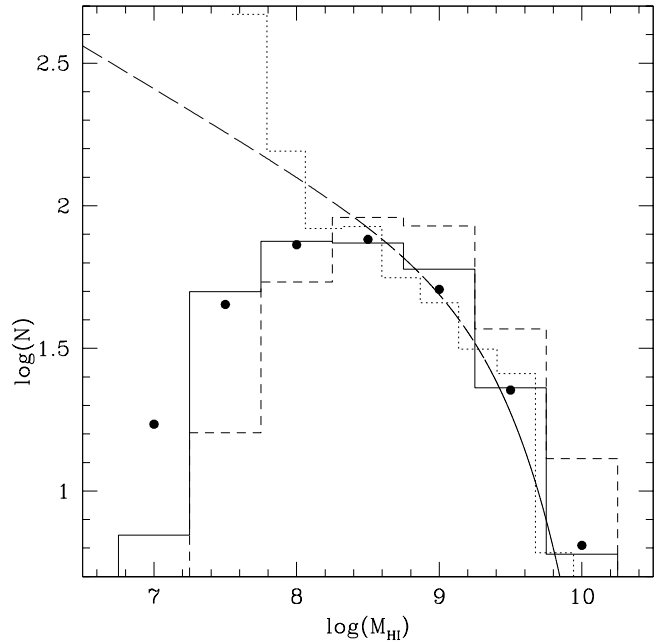


Fig. 6. The dotted histogram is obtained from the late-type galaxies optical luminosity function, as determined in the field by Marzke et al. (1998), transformed into M_{HI} using the relation $\log M_{HI} = 2.9 - 0.34 \times M_p$ discussed in the text. It appears consistent with the field HILF of Zwaan et al. (2003) (long dashed line) indicating that most of the HI is contributed to by late-type galaxies. The dashed histogram is obtained from the late-type galaxies optical luminosity function of Virgo (see Fig 7), transformed into M_{HI} using the same M_{HI} vs. M_p relation. The continuum histogram is the HIMF actually observed in Virgo (see Fig. 5). The filled dots represent the Montecarlo simulation described in the text aimed at modeling the effects of the H I deficiency on the HIMF.

minosity in a population of isolated, unperturbed galaxies (taken from GOLDmine), we transform the optical luminosity function of field S+Im galaxies by Marzke et al. (1998) into an HILF_{S+Im}, as shown by the dotted histogram of Fig. 6. The actual measured HILF obtained by Zwaan et al. (2003) is consistent with the HILF_{S+Im}, at least for $M_{HI} > 10^{7.5}$ M \odot .

Similarly we transform the optical luminosity function of Virgo (Fig. 7) into the HILF_{S+Im} (dashed histogram in Fig. 6) and compare it to the measured HILF (continuum histogram). The two are in general agreement, with some noticeable differences: the HILF_{S+Im} is in excess over the measured HILF in the range $M_{HI} > 10^9$ M \odot , while it lies below the measured HILF for $M_{HI} < 10^8$ M \odot . Both discrepancies can be understood in terms of H I deficiency. Massive spirals in Virgo have large Def_{HI} parameters that shift their measured M_{HI} one or two decades below the corresponding values for isolated spirals, producing the measured HILF excess over the HILF_{S+Im} at $M_{HI} < 10^8$ M \odot . Solanes et al. (2001) found that the dis-

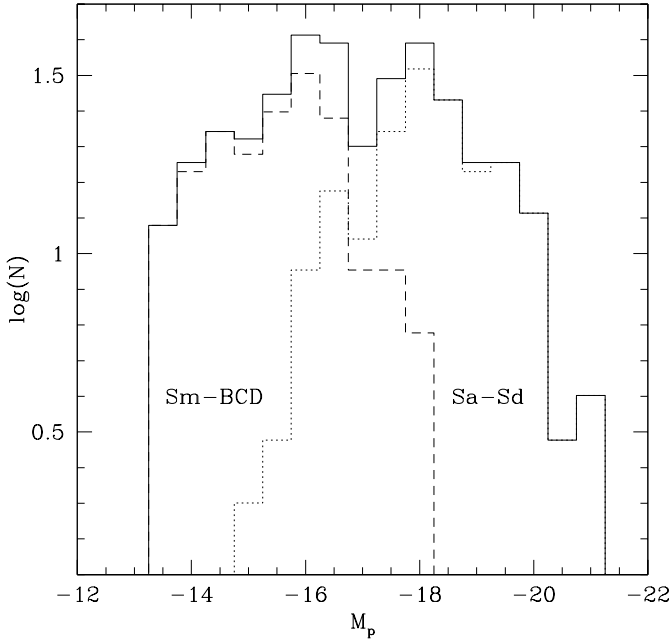


Fig. 7. The optical luminosity distribution of the 355 late-type galaxies analyzed in this work, divided in Giants and Dwarfs, consistent with the one in Sandage et al. (1985) for $m_p \leq 18.0$ mag, accounting for the different assumed distance.

tribution of HI deficiency among galaxies of latest types in the Virgo cluster is skewed toward high values. This can be either due to a real higher than average gas depletion or to the poorly calibrated deficiency parameter for these systems, as mentioned earlier. However Hoffman et al. (1985) confirm that the HI (hybrid) surface brightness is monotonously decreasing toward later Hubble types and fainter optical luminosities. Disregarding these second order dependences of the HI deficiency parameter on the Hubble type at extreme low luminosities, we have simulated the first order effect of the HI deficiency on the HIMF by running a Montecarlo simulation with the simple assumption that the Def_{HI} parameter of galaxies in the Virgo cluster is Gaussian distributed with a mean of 0.4 and a FWHM of 0.8, independent of the galaxy luminosity. Starting from the optical luminosity function of S+Im of Fig. 7 and assuming the $\log M_{HI} = 2.9 - 0.34 \times M_p$ relationship we have been able to reproduce (filled dots) the observed HIMF (continuum histogram) of Fig. 6.

5.4. The HIMF adopting upper limits

So far we have shown that the HI mass function obtained from HI follow-up observations of an optically selected sample of late-type galaxies is in agreement with the HIMF derived from a blind HI survey. We have however not considered the relatively minor contribution from the upper limits, i.e. 59/355 galaxies that were surveyed but not detected.

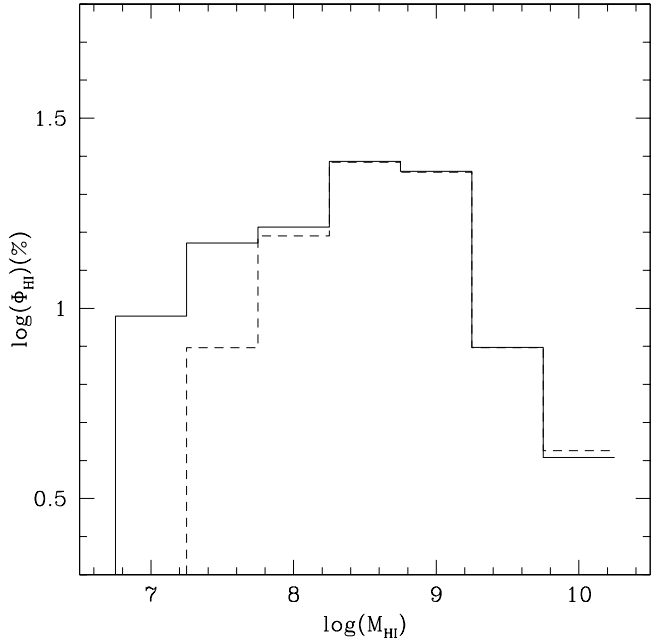


Fig. 8. The fractional HI mass function as derived from the detected objects alone (dashed histogram) and including undetected galaxies (continuum histogram).

Radio astronomers have developed a robust method to account for upper limits when deriving the continuum radio luminosity function (Avni et al. 1980; see a recent application to Virgo in Gavazzi & Boselli 1999) that we apply to the HI data. Fig. 8 shows that the fractional HIMFs derived with (continuum histogram) and without (dashed histogram) taking into account the contribution from upper limits are identical above $\log M_{HI} = 8 M_\odot$. Upper limits contribute for smaller masses, and make the faint-end slope of the HIMF less steep. This is a small difference that should however not be disregarded.

6. Conclusions

We have observed in the 21-cm H_I line, with the refurbished Arecibo telescope, 33 galaxies in the Virgo cluster. Given the high sensitivity of our observations (rms noise ~ 0.5 mJy corresponding to $\log M_{HI} = 6.6 M_\odot$) 12 objects were detected and stringent upper limits were obtained for the remaining ones.

In the Virgo area covered by the VCC the new observations brought to 100 % completeness the HI survey of late-type galaxies with $m_p \leq 18.0$ mag which are cluster members or bona-fide members.

Using the Virgo HI data set, comprising 355 late-type galaxies (296 of which are positive detections) we construct the cluster HI mass function (HIMF) as derived from an optically selected HI survey. Considering or disregarding the contribution from HI non-detections, we find it in remarkable agreement with the radio selected HIMF available for this cluster from Davies et al. (2004).

The low-mass end of the Virgo HIMF is inconsistent with the field HIMF of Zwaan et al. (2003).

We show that both the Virgo and the field HIMFs can be obtained from the optical luminosity function of S+Im galaxies alone, under the assumption that M_{HI} scales with M_p according to the universal relation: $\log M_{HI} = 2.9 - 0.34 \times M_p$.

The latter evidence allows us to conclude that neutral hydrogen in the local universe is primarily contributed by late-type galaxies, with marginal contributions from early-type galaxies and isolated H_I clouds.

The inconsistency between the cluster and the field HIMF derives primarily from the difference in the optical luminosity function of late-type galaxies in the two environments and from the HI deficiency occurring in spirals in rich clusters.

Acknowledgements. We thank Luca Cortese for running the Montecarlo simulations and for useful discussions. The Arecibo Observatory is part of the National Astronomy and Ionosphere Center, which is operated by Cornell University under a cooperative agreement with the National Science Foundation. This research also has made use of the Goldmine database, of the Lyon-Meudon Extragalactic Database (Leda), recently incorporated in HyperLeda and of the NASA/IPAC Extragalactic Database (NED) which is operated by the Jet Propulsion Laboratory, California Institute of Technology, under contract with the National Aeronautics and Space Administration.

References

- Avni Y., Soltan A., Tananbaum H., & Zamorani C., 1980, ApJ, 238, 800
 Binggeli, B., Sandage, A., & Tammann, G. A., 1985, AJ, 90, 1681 (VCC)
 Binggeli, B., Popescu, C., & Tammann, G. A., 1993, A&AS, 98, 275
 Börhringer, H., Briel, U. G., Schwarz, R. A. et al., 1994, Nature, 368, 828
 Bottinelli, L., Gouguenheim, L., & Paturel, G., 1982a, A&A, 113, 61
 Byrd, G., & Valtonen, M., 1990, ApJ, 350, 89
 Cayatte, V., van Gorkom, J., Balkowski, C., & Kotanyi, C., 1990, AJ, 100, 604 (CG90)
 Cayatte, V., Kotanyi, C., Balkowski, C., & van Gorkom, J., 1994, AJ, 1007, 103
 Chamaraux, P., Balkowski, C., & Gerard, E. 1980, A&A, 83, 38
 Chincarini, G., Giovanelli, R., & Haynes, M. P., 1983, ApJ, 269, 13
 Cowie, L.L., & Songaila, A., 1977, Nature, 266, 501
 Davies, J., Minchin, R., Sabatini, S., et al., 2004, MNRAS, 349, 922 (D04)
 Falco, E. E., Kurtz, M. J., Geller, M. J., et al., 1999, PASP, 111, 438
 Gavazzi, G., 1987, ApJ, 320, 96
 Gavazzi, G., 1989, ApJ, 346, 59
 Gavazzi, G., & Boselli, A., 1999, A&A, 343, 86
 Gavazzi, G., Pierini, D., & Boselli, A., 1996, A&A, 312, 397
 Gavazzi, G., Carrasco, L., & Galli, R., 1999a, A&AS, 136, 227
 Gavazzi, G., Boselli, A., Scodéggi, M., Pierini, D., & Belsole, E., 1999b, MNRAS, 304, 595
 Gavazzi, G., Boselli, A., Pedotti, P., Gallazzi, A., & Carrasco, L., 2002, A&A, 396, 449
 Gavazzi, G., Boselli, A., Donati, A., Franzetti, P., & Scodéggi, M., 2003, A&A, 400, 451
 Gavazzi, G., Cortese, L., Boselli, A., et al., 2003, ApJ, 597, 210
 Giovanardi, C., Krumm, N., & Salpeter, E.E., 1983, AJ, 88, 1719 (GK83)
 Giovanardi, C., & Salpeter, E.E. 1985, A&AS, 58, 623
 Giovanelli, R., & Haynes, M., 1985, ApJ, 292, 404
 Gregory, S., Tifft, W., & Moody, W., 1988, AJ, 95 662
 Gunn, J.E., & Gott, J. R.III, 1972, ApJ, 176, 1
 Haynes, M. & Giovanelli, R., 1984, AJ, 89, 758
 Haynes, M., Giovanelli, R., & Chincarini, G., 1984, ARA&A, 22, 445
 Haynes, M. & Giovanelli, R., 1986, ApJ, 306, 466 (HG86)
 Helou, G., Hoffman, G. , & Salpeter, E., 1984, ApJS, 55, 433 (HH84)
 Helou, G., Salpeter, E., Giovanardi, C., & Krumm, N., 1981, ApJS, 46, 267 (HS81)
 Helou, G., Salpeter, E. & Terzian, Y., 1982, AJ, 87, 1443 (HS82)
 Hewitt, J. N., Haynes, M. P., & Giovanelli, R., 1983, AJ, 88, 272
 Hoffman, G. L., Helou, G., Salpeter E.E., & Sandage, A., 1985, ApJ, 298, L15
 Hoffman, G. L., Helou, G., Salpeter E.E., Glosson, J., & Sandage, A., 1987, ApJS, 63, 247 (HH87)
 Hoffman, G.L., Lewis, B.M., Helou, G., Salpeter, E.E., & Williams, H.L., 1989a, ApJS, 69, 65 (HL89)
 Hoffman, G. L., Williams, H., Salpeter, E.E., Sandage, A., & Binggeli, B., 1989, ApJS, 71, 701 (HW89)
 Hoffman, G.L., Lewis, B.M., & Salpeter, E.E., 1995, ApJ, 441, 28 (HL95)
 Hoffman, G.L., Brosch, N., Salpeter, E.E., & Carle, N.J., 2003, AJ, 126, 2774 (HB03)
 Huchtmeier, W.K., 1982, A&A, 110, 121
 Huchtmeier, W.K., & Richter, O.G., 1986, A&AS, 64, 111 (HR86)
 Huchtmeier, W., & Richter, O., 1989, A General Catalogue Of Hi Observations Of External Galaxies, New York, Springer-Verlag (HR89)
 Krumm, N., & Salpeter, E.E., 1979, ApJ, 227, 776
 Lewis B.M., 1985, ApJ, 292, 451
 Magri, C., 1994, AJ, 108, 896 (M94)
 Marzke, R.O., da Costa, L.N., Pellegrini, P.S., Willmer, C.N.A. & Geller, M.J., 1998, ApJ, 503, 617
 Merritt, D., 1983, ApJ, 264, 24
 Mirabel, F., & Wilson, A.S., 1984, ApJ, 277, 92
 Moore, B., Katz, N., Lake, G., Dressler, A., & Oemler, A., Jr. 1996, Nature, 379, 613
 Nulsen, P.E.J., 1982, MNRAS, 198, 1007
 O'Neil, K., 2004, AJ, (in press), astro-ph/040811.
 Peterson S., 1979, ApJS, 40, 527 (P79)
 Sakai, S., Kennicutt, R.C.Jr., van der Hulst, J.M., & Moss, C., 2002, ApJ, 578 , 842
 Salpeter, E.E., & Hoffman, G. L., 1996, ApJ, 465, 595
 Sandage, A., Binggeli, B., & Tammann, G.A., 1985, AJ, 90, 1759
 Schneider, S.E., Helou, G., Salpeter, E.E., & Terzian, Y., 1986, AJ, 92, 742
 Schneider, S.E., Thuan T.X., Magri, C., & Wadiak, J.E., 1990, ApJS, 72, 245 (SS90)
 Schneider, S.E., Thuan, T.X., Mangum, J.G., & Miller, J., 1992, ApJS, 81, 5

- Solanes, J., Giovanelli, R., & Haynes, M., 1996, ApJ, 461, 609
Solanes, J. et al., 2001, ApJ, 548, 97.
Strauss, M.A., Huchra, J.P., Davis, M., et al. 1992, ApJS, 83,
29
Sulentic, J., & Arp, H., 1982, AJ, 88, 489 (SA82)
Sullivan III, W.T., Bates, B., Bothun, G.D., & Schommer,
R.A., 1981, AJ, 86, 919
Tully, B., & Fisher, J., 1977, A&A, 54, 661
Tully, B., & Shaya, E., 1984, ApJ, 281, 31
van Driel, W., Ragaigne, D., Boselli, A., Donas, J., & Gavazzi,
G., 2000, A&AS, 144, 463 (DR00)
Warmels, R., 1986, Ph.D. Thesis, Groningen University (W86)
Zwaan, M. A., et al. 2003, AJ, 125, 2842

Table 1 Parameters of the newly observed galaxies.

Obj.	RA (J2000.0)	Dec	V_{opt} (km/s)	σ (mJy)	S_p (mJy)	V_{HI} (km/s)	W_{50} (km/s)	W_{20} (km/s)	I_{HI} (Jy km/s)	Qual.
Virgo Cluster										
VCC 1	120820.02	134100.2	2275±43	0.34	1.6	2240±5	107	124	0.13±0.03	2
VCC 48	121215.11	122917.8	-52±60	0.64	-	-	-	-	-	-
VCC 99	121402.18	064323.3	2454±44	0.72	6.1	2418±4	169	189	0.72±0.08	1
VCC 222	121709.83	071129.1	2298±122	0.60	-	-	-	-	-	-
VCC 227	121714.38	085632.1	1290±60	0.34	1.2	1304:±7	24	41	0.02±0.02	4
VCC 256	121747.74	042838.3	2103±60	0.44	1.7	2007:±40	307	410	0.31±0.07	4
VCC 275	121811.29	093002.4	1733±60	0.54	-	-	-	-	-	-
VCC 315	121900.46	060540.7	1594±46	0.57	-	-	-	-	-	-
VCC 323	121906.39	054332.7	2759±35	0.53	-	-	-	-	-	-
VCC 341	121922.15	060554.8	1827±60	0.76	-	-	-	-	-	-
VCC 358	121935.66	055047.9	2599±59	28	-	-	-	-	-	-
VCC 362	121942.19	053216.9	156±44	0.44	-	-	-	-	-	-
VCC 517	122201.37	050603.8	1888±51	0.37	3.4	1864±12	285	356	0.37±0.06	1
VCC 524	122205.74	090238.8	1117±98	0.51	5.1	1035±1	322	329	1.14±0.07	1
VCC 528	122207.76	060611.8	7019±60	0.63	5.2	7046±9	261	309	0.86±0.09	1
VCC 531	122210.88	045705.9	1912±60	0.56	-	-	-	-	-	-
VCC 666	122346.13	164728.5	-	0.51	-	-	-	-	-	-
VCC 675	122354.35	030504.6	1860±42	0.78	14.0	1857±	91	128	1.14±0.07	2
VCC 679	122355.17	112928.6	-	1.19	-	-	-	-	-	-
VCC 802	122529.01	132947.3	-215±42	0.58	-	-	-	-	-	-
VCC 1086	122816.00	092610.6	294±39	0.63	6.7	328±8	240	294	0.93±0.09	3
VCC 1121	122841.73	110754.9	-	0.66	-	-	-	-	-	-
VCC 1189	122928.83	064612.3	544±43	1.17	49.5	516±1	112	132	4.17±0.11	1
VCC 1196	122931.25	140258.3	908±36	0.57	-	-	-	-	-	-
VCC 1237	122951.15	135203.5	-335±60	0.77	-	-	-	-	-	-
VCC 1287	123023.79	135855.8	-	0.72	-	-	-	-	-	-
VCC 1358	123122.99	171223.3	-	0.66	-	-	-	-	-	-
VCC 1377	123139.21	105008.5	-	0.51	-	-	-	-	-	-
VCC 1435	123232.42	080239.0	609±42	0.44	-	-	-	-	-	-
VCC 1448	123240.83	124613.1	-	0.92	-	-	-	-	-	-
VCC 1597	123502.77	052534.6	861±60	0.39	5.4	841±2	124	144	0.51±0.04	1
VCC 1885	124137.57	154933.2	-	0.38	-	-	-	-	-	-
VCC 1970	124329.11	100534.7	1325±60	0.37	3.0	1324±12	70	136	0.13±0.03	3

Table 2: Basic H_I properties of late-type Virgo galaxies.

VCC (1)	Type (2)	m_p (mag) (3)	a (arcmin) (4)	Cloud (5)	V km s ⁻¹ (6)	$\log M_{HI}$ (M_\odot) (7)	Def_{HI} (8)	Qual (9)	Ref. (10)
1	BCD	14.78	0.80	M	2240	7.50	1.14	2	T.W.
4	Im	17.50	0.50	M	589	8.25	0.00	2	HH87
10	BCD	14.75	1.03	M	1973	8.77	0.08	1	HH87
15	Sa	14.70	1.37	M	2545	8.55	0.43	1	HL89
17	Im	15.20	0.91	M	819	8.78	-0.04	2	HH87
22	BCD	16.00	0.27	M	1695	8.23	-0.49	2	HB03
24	BCD	14.95	1.00	M	1292	8.96	-0.15	1	HB03
25	Sc	12.46	2.54	M	2169	9.73	-0.21	1	M94
26	Im	17.50	0.43	M	2469	8.38	-0.26	3	HH87
34	Sc	14.65	1.16	M	266	8.99	-0.12	1	HL89
47	Sa	14.20	1.41	M	1862	8.39	0.61	1	HG86
48	Sdm	14.30	1.71	M	-52	< 7.29	1.97	-	T.W.
52	Im	17.80	0.39	W	2088	7.64	0.42	5	HH87
58	Sb	13.17	2.54	M	2207	9.46	0.11	1	HH84
66	Sc	11.89	5.35	N	369	9.81	-0.20	1	W86
67	Sc	13.98	2.26	M	-183	9.17	0.25	1	HL89
73	Sb	13.35	1.89	W	2082	8.96	0.40	2	HL89
74	BCD	16.30	0.85	N	861	< 7.02	1.15	-	HH87,D04*
79	Im	17.20	0.57	N	-	< 7.12	0.73	-	HH87,D04
81	Sc	15.60	0.95	N	2075	8.63	-0.45	1	HG86,D04*
83	Im	15.13	1.26	N	2439	8.04	0.46	1	HH87,D04*
87	Sm	15.00	1.45	N	-134	8.32	0.29	2	HH87,D04

Table 2: Continue

VCC	Type	m_p (mag)	a (arcmin)	Cloud	V km s ⁻¹	$\log M_{HI}$ (M_\odot)	Def_{HI}	Qual	Ref.
89	Sc	12.53	2.26	M	2116	9.46	-0.03	1	HH84,D04*
92	Sb	10.92	9.78	N	-135	9.76	0.33	1	HR89,D04
97	Sc	13.20	1.96	M	2476	9.08	0.23	1	M94,D04*
99	Sa	14.81	1.41	W	2418	8.24	0.77	1	T.W.
105	Sd	13.68	2.48	W	1221	9.27	0.29	1	HL89
114	Im	16.00	0.64	W	2071	8.70	-0.24	2	HH87
117	Im	16.50	0.64	W	1788	8.93	-0.47	1	HH87
119	Sc	14.76	1.71	M	620	9.04	0.15	1	HL89,D04*
120	Scd	13.47	3.60	W	2064	9.70	0.17	1	HH84
124	Sm	16.00	0.71	M	2084	7.73	0.81	3	HH87,D04*
126	Sd	14.42	1.87	N	263	8.50	0.32	1	HL89,D04
130	BCD	16.50	0.63	N	2189	7.86	0.06	1	HH87
131	Sc	14.34	2.60	N	2317	8.93	0.09	1	HG86,D04*
132	Sd	16.40	1.36	N	2085	8.11	0.44	2	HL89,D04*
135	S/BCD	14.81	1.16	M	2378	< 7.19	1.75	-	HG86,D04*
143	Sc	15.46	1.00	N	375	7.88	0.35	1	HL89,D04
144	BCD	15.31	0.63	W	2014	8.74	-0.31	2	HH87
145	Sc	12.77	5.10	N	702	9.39	0.19	1	HH84,D04*
152	Scd	13.48	1.96	N	592	8.61	0.24	1	HL89
157	Sc	11.50	3.60	N	-83	8.68	0.61	1	HH84,D04
159	Im	15.08	1.04	W	2584	8.55	0.30	2	HH87
162	Sd	14.41	2.92	N	1979	8.88	0.30	1	HL89
167	Sb	10.97	9.12	N	140	9.35	0.69	1	CG90,D04
168	Im	17.10	0.43	N	682	7.35	0.26	2	HH87,D04*
169	Im	16.50	0.85	N	2222	8.52	-0.35	2	HH87
170	Sd	14.56	1.16	N	1411	7.45	0.98	2	HG86,D04*
171	Im	17.40	0.57	W	875	7.16	1.20	4	HW89
172	BCD	14.50	1.26	W	2175	9.06	-0.05	-	HH87
187	Scd	13.91	3.52	N	226	8.93	0.40	1	HH84,D04
199	Sa	12.95	2.92	W	2594	8.81	0.72	1	M94
207	BCD	17.20	0.36	W	2564	8.25	-0.25	2	HW89
213	S/BCD	14.26	0.93	N	-162	8.00	0.25	2	HG86,D04
217	Im	15.50	1.71	N	1183	8.61	0.14	2	HG86
221	Sc	13.43	1.76	W	2031	8.81	0.41	2	HL89
222	Sa	12.62	4.33	W	2298	< 7.81	1.99	-	T.W.
223	BCD	16.50	0.34	W	2070	8.22	-0.29	2	HH87
224	Scd	14.70	1.87	N	2133	8.62	0.20	1	HG86,D04*
226	Sc	12.53	2.01	N	864	8.32	0.48	1	M94,D04*
227	Sdm	14.90	1.16	W	1304	6.68	2.25	3	T.W.
234	Sa	12.99	3.36	W	2237	8.37	1.26	1	M94
241	Sd	14.60	2.60	N	-163	8.72	0.36	1	HG86,D04
260	Im	15.70	1.03	W	1775	8.03	0.82	2	HH87
267	Sbc	13.82	2.01	B	733	9.04	0.15	1	HL89
274	BCD	17.50	0.57	W	-	< 7.49	0.87	-	HW89
275	Im	14.54	1.79	W	1733	< 7.22	2.08	-	T.W.
280	Im	17.70	0.28	N	-	< 6.89	0.38	-	HH87
281	S/BCD	15.38	0.14	N	257	7.58	-0.91	2	HH87,D04
286	Im	16.00	0.51	W	1822	7.93	0.35	3	HH87
289	Sc	14.81	1.71	W	863	8.89	0.30	1	HL89
297	Sc	15.10	1.16	B	1999	8.27	0.32	1	HL95
307	Sc	10.43	6.15	N	2405	9.71	0.01	1	HS81,D04*
309	Im/BCD	16.20	0.64	N	1566	7.71	0.23	2	HH87,D04*
313	Sa	14.62	1.26	W	2376	8.78	0.14		HR86 3
315	Sa	14.98	1.10	W	1594	< 7.79	1.04	-	T.W.
318	Scd	14.01	1.71	W	2469	9.39	-0.13	1	HL89
322	Im	15.10	1.26	N	-206	8.25	0.25	2	HG86,D04
323	Sa	14.91	1.16	W	2759	< 7.76	1.10	-	T.W.
324	BCD	14.78	1.35	S	1524	8.19	0.36	2	HH87
328	Im	16.90	1.00	N	2179	7.98	0.33	2	HG86,D04*
329	Im	16.80	0.63	B	1622	7.98	0.19	2	HH87
331	Pec	15.00	1.00	W	1984	8.13	0.89	3	HL95
334	BCD	15.87	0.56	N	-254	7.95	-0.11	2	HH87,D04
340	BCD	14.43	1.10	W	1512	8.82	0.08	2	HH87
341	Sa	12.70	3.52	B	1827	< 7.63	1.79	-	T.W.
343	Sd	15.10	1.10	B	2479	7.98	0.65	2	HL89
350	Im	17.05	0.66	N	305	7.97	-0.01	3	HH87,D04
358	Sa	13.80	1.55	B	2599	< 8.65	0.18	-	HR86
362	Sa	14.51	2.16	W	156	< 7.68	1.63	-	T.W.
364	Im	17.30	0.74	N	-	< 7.05	1.00	-	HH87,D04
367	Im	17.20	0.56	W	2350	7.99	0.37	1	T.W.
381	Im	16.50	0.85	B	482	8.25	0.17	2	HH87
382	Sc	12.37	2.01	W	2378	9.65	-0.32	1	HH84
386	Sa	14.47	1.55	W	2380	9.25	-0.18	1	DR00
393	Sc	13.25	2.10	B	2617	8.76	0.33	1	HL89
404	Scd	15.00	1.71	S	1733	8.34	0.41	1	HL89
410	BCD	17.10	0.31	N	284	7.38	-0.03	3	HH87,D04
415	Sd	14.82	1.16	B	2560	8.28	0.39	1	HL89
423	Im	17.30	0.51	S	2384	8.06	-0.30	1	HW89
425	Im	17.30	0.43	B	-	< 6.98	0.87	-	HW89
428	BCD	17.50	0.39	A	794	7.63	-0.08	2	HH87,D04*
446	Im/BCD	15.50	0.85	B	825	7.68	0.74	3	HH87

Table 2: Continue

VCC	Type	m_p (mag)	a (arcmin)	Cloud	V km s ⁻¹	$\log M_{HI}$ (M_\odot)	Def_{HI}	Qual	Ref.
448	Im	16.80	0.39	A	672	7.79	-0.25	2	HH87,D04*
449	Sbc	14.34	4.33	S	2541	9.02	0.51	1	HL89
453	Sm	16.00	0.79	N	910	7.71	0.41	2	HH87
459	BCD	14.95	0.84	A	2108	8.22	-0.07	2	HH87,D04*
460	Sa	11.20	5.10	A	921	7.62	1.85	3	M94,D04*
464	BCD	17.50	0.64	B	-	< 7.05	1.14	-	HW89
465	Sc	12.62	3.95	N	357	9.26	0.10	1	HH84
467	Im	17.70	0.43	S	2435	7.58	0.03	1	HW89
468	BCD	16.00	0.56	S	1980	7.68	0.16	2	HB03
476	Im	17.90	0.36	N	-	< 7.09	0.40	-	HW89
477	Im	16.96	1.00	A	1866	7.53	0.77	3	HH87,D04*
483	Sc	12.08	3.60	A	1136	8.94	0.34	3	HH84,D04*
491	Scd	12.86	1.96	N	234	9.14	-0.29	1	HH84
492	Sa	13.76	2.16	B	2310	< 7.79	1.28	-	HL89
497	Sc	12.55	6.74	A	1150	9.24	0.56	1	HH84,D04*
508	Sc	10.17	6.59	S	1568	9.85	-0.06	1	HH84
509	Sdm	14.98	1.45	B	1258	8.47	0.38	1	HH87
512	Sm	15.69	1.45	A	153	8.40	0.21	1	HH87
513	BCD	15.10	0.73	S	1832	7.27	0.79	2	HH87
514	Sc	14.70	1.41	B	851	8.12	0.65	2	HL89
517	Sab	14.90	1.00	S	1864	7.40	0.91	1	T.W.
520	Im	17.50	0.50	B	-	< 7.43	0.55	-	HW89
522	Sa	13.19	2.60	A	1888	< 7.44	1.55	-	GK83,D04*
524	Sbc	12.79	3.95	B	1035	8.15	1.53	1	T.W.
530	Im	15.80	1.29	A	1297	7.60	0.91	2	HH87,D04*
531	Sa	15.00	1.10	S	1912	< 7.24	1.14	-	T.W.
534	Sa	13.59	2.01	B	1071	7.64	1.38	3	M94
552	Sc	13.61	1.89	S	1296	9.17	-0.42	1	HL89
559	Sab	12.56	5.10	A	153	8.09	1.38	1	HH84,D04
562	BCD	16.20	0.63	A	44	< 7.02	0.90	-	HH87,D04
565	Im	15.70	0.93	B	877	7.77	0.73	2	HH87
566	Sm	15.80	0.71	B	1407	8.59	-0.32	2	HH87
567	Scd	14.36	2.16	B	2366	8.82	0.36	2	HL89
570	Sab	12.73	5.10	A	1443	8.11	1.36	1	HH84
576	Sbc	13.70	2.48	B	1254	9.20	0.15	1	HG86
583	Im	15.76	1.16	A	-72	< 7.12	1.31	-	HH87,D04
584	Im	15.80	0.71	B	56	7.00	1.27	5	HH87
585	Im	17.00	1.16	A	-	< 7.09	1.34	-	HH87
596	Sc	10.11	9.12	A	1575	9.52	0.53	1	HS81,D04*
613	Sa	12.60	3.52	S	1670	8.83	0.38	1	HW89
618	Im	16.50	0.60	A	1890	7.94	-0.05	2	HH87,D04*
620	Sm	15.20	1.26	A	746	8.02	0.48	2	HG86
630	Sd	13.10	5.86	A	1564	8.59	1.16	1	HH84
641	BCD	15.08	0.73	B	906	8.15	0.15	3	HH87
655	S/BCD	13.21	1.55	A	1147	7.91	0.75	2	GK83,D04*
656	Sb	13.14	2.48	B	1014	8.79	0.53	1	HH84
664	Sc	13.50	2.60	A	-427	8.40	0.62	2	HS81,D04
666	Im	16.80	1.00	A	-	< 6.65	1.66	-	T.W.,D04
667	Sc	14.24	1.71	B	1420	8.34	0.58	1	HL89
675	Sa	15.00	0.56	S	1857	7.89	0.01	2	T.W.
688	Sc	13.94	1.41	B	1125	8.32	0.45	1	HL89
692	Sc	12.93	2.92	A	2324	8.46	0.66	1	HS81,D04*
693	Sm	15.06	1.16	S	2048	8.10	0.32	1	HH87
697	Sc	14.17	1.55	B	1231	8.22	0.62	2	HL89
699	Pec	14.22	1.95	B	727	9.03	0.19	2	HL89
713	Sc	14.04	3.20	B	1137	8.10	1.34	3	HG86
737	S/BCD	14.94	1.07	S	1725	8.46	-0.09	1	HH87
739	Sd	14.37	2.01	S	927	8.78	0.10	2	HL89
740	Sm	15.70	0.71	B	875	8.19	0.08	2	HH87
741	BCD	15.50	0.84	S	1861	8.04	0.12	1	HH87
768	Sc	14.91	1.03	A	2434	8.09	0.16	1	HL89,D04*
772	BCD	17.00	0.51	S	1226	7.67	0.09	2	HH87
785	Sa	12.16	3.06	S	2557	9.00	0.10	1	HH84
787	Scd	13.69	1.84	B	1136	8.79	0.26	1	SS90
792	Sab	12.36	3.52	B	971	8.57	0.85	1	HH84
793	Im	16.74	0.47	A	1906	7.65	0.05	2	HH87,D04*
802	BCD	17.40	0.64	A	-215	< 6.70	1.24	-	T.W.,D04
809	Sc	14.55	1.45	A	-142	8.39	0.15	2	HG86,D04
825	Im	15.90	1.00	B	-	< 7.16	1.40	-	HH87
826	Im	15.00	1.20	S	1507	8.32	0.14	2	HH87
827	Sc	13.76	3.60	B	992	9.45	0.08	1	HL89
836	Sab	11.83	5.10	A	2515	8.78	0.69	1	HS81,D04*
841	BCD	15.60	0.84	A	501	7.61	0.55	2	HG86,D04*
848	Im/BCD	14.72	1.16	B	1537	8.85	-0.18	2	HH87
849	Sbc	13.27	2.18	B	1103	8.84	0.41	1	SA82
851	Sc	14.14	2.16	B	1195	8.88	0.23	1	HG86
857	Sb	11.76	3.60	A	914	8.51	0.86	1	HS81,D04*
859	Sc	14.61	2.92	S	1428	8.62	0.49	1	HL89
865	Sc	13.02	3.36	A	-124	8.85	0.38	1	SS90,D04
873	Sc	12.56	3.95	A	234	8.74	0.63	1	HH84,D04
874	Sc	12.99	1.89	A	1738	7.81	0.95	3	M94,D04*

Table 2: Continue

VCC	Type	m_p (mag)	a (arcmin)	Cloud	V km s ⁻¹	$\log M_{HI}$ (M_\odot)	Def_{HI}	Qual	Ref.
888	Im	15.78	1.16	B	1090	8.25	0.41	2	HH87
890	BCD	16.00	0.21	B	1483	7.33	-0.05	2	HW89
905	Sc	13.42	2.79	B	1290	8.97	0.35	2	HL89
912	Sbc	12.97	2.92	A	105	8.26	0.99	1	HS81,D04
921	Sbc	13.14	1.89	S	2289	8.33	0.59	2	HL89
938	Sc	13.28	2.18	S	1395	8.52	0.36	1	HH84
939	Sc	12.92	3.45	B	1271	9.26	0.24	2	HL89
945	Sm	15.31	1.29	A	-9	8.21	0.31	3	HH87,D04
950	Sm	14.49	1.71	A	1098	8.81	-0.07	2	HH87
952	Im	16.50	0.78	B	985	8.12	0.23	2	HL89
957	Sc	12.67	2.01	S	1695	8.79	0.02	1	M94
958	Sa	12.13	3.52	A	-273	8.06	1.14	1	GK83,D04
963	Im	17.20	0.50	A	1866	7.73	0.01	3	HH87,D04*
971	Sd	14.28	3.06	B	1120	9.26	0.20	2	HW89
975	Scd	13.58	3.95	B	933	9.34	0.33	1	HL89
979	Sa	12.32	4.33	B	438	8.40	1.17	2	GK83
980	Scd	14.17	2.48	A	2342	8.38	0.67	1	HL89,D04*
984	Sa	12.82	2.99	A	1883	< 7.31	1.78	-	GK83,D04*
985	BCD	17.00	0.63	S	1638	7.31	0.61	3	HH87
989	Sc	15.80	0.67	S	1846	7.50	0.41	3	HH87
995	Sc	15.32	1.53	A	928	8.92	-0.33	1	HG86
1001	Im	16.60	0.73	A	338	7.49	0.57	3	HH87,D04
1002	Sc	12.48	3.02	B	1450	8.92	0.47	1	HH84
1011	Sdm	14.85	1.29	S	874	8.08	0.43	1	HH87
1013	Im	16.71	0.73	B	1712	7.51	0.79	4	HH87
1017	Im	14.50	2.16	B	32	< 7.10	2.07	-	HH87
1021	Im	15.45	1.16	B	868	7.64	1.03	4	HH87
1043	Sb	10.91	8.12	A	70	8.62	1.33	2	GK83,D04
1047	Sa	12.48	2.01	A	724	< 7.44	1.37	-	GK83,D04*
1048	Scd	15.10	1.71	B	2252	8.43	0.56	1	HL89
1060	Sm	15.00	1.07	S	1487	8.10	0.27	2	HH87
1091	Sbc	14.60	1.45	B	1119	9.30	-0.35	1	HG86
1102	Im	17.70	0.35	S	-	< 7.17	0.29	-	HW89
1106	Im	17.50	0.59	A	-	< 6.64	1.23	-	HH87
1110	Sab	10.93	6.15	A	1954	8.65	0.95	1	HH84,D04*
1114	Im	14.82	1.71	S	560	7.28	1.46	4	HH87
1118	Sc	13.31	1.96	B	865	8.52	0.51	1	HL89
1121	Im	16.48	0.71	A	-	< 6.76	1.26	-	T.W.
1126	Sc	13.30	2.92	A	1687	7.78	1.33	1	HL89,D04*
1128	Im	17.34	0.71	B	-	< 7.24	1.02	-	HH87
1141	BCD	16.20	0.46	B	1040	7.84	0.07	3	HH87
1145	Sb	11.66	2.92	S	884	8.35	0.86	2	GK83
1156	Scd	14.13	2.48	S	1576	8.82	0.23	1	HL89
1158	Sa	12.09	3.52	A	1919	< 7.13	2.07	-	M94,D04*
1166	Im	17.70	0.71	A	-	< 7.12	0.90	-	HH87,D04
1168	Im	17.70	0.43	B	-	< 7.41	0.45	-	HW89
1169	Im	17.80	0.28	A	-	< 6.94	0.33	-	HW89,D04
1179	Im/BCD	15.58	1.16	B	765	7.73	0.94	4	HH87
1189	Sc	13.70	1.84	S	516	8.45	0.28	1	T.W.
1190	Sa	12.22	4.33	B	508	< 7.64	1.93	-	GK83
1193	Sc	14.62	1.20	S	757	8.43	-0.05	1	HG86
1200	Im	15.10	1.26	A	-123	< 6.84	1.65	-	HH87
1205	Sc	13.04	1.84	S	2339	8.76	-0.03	1	HH84
1208	Im	15.20	0.84	S	1337	7.64	0.52	2	HH87
1217	Sm	14.59	1.87	A	38	< 6.54	2.28	-	HW89
1249	Im	14.75	1.45	S	468	7.06	1.55	4	HH87
1257	Im	16.50	1.36	A	2488	8.41	0.14	1	HH87,D04*
1266	Sdm	14.63	1.16	S	1637	8.24	0.19	2	HH87
1273	Im	15.25	1.16	B	2015	< 7.16	1.51	-	HH87
1287	Im	16.00	0.85	A	-	< 6.80	1.38	-	T.W.
1290	Sb	13.09	2.01	S	2438	8.90	0.05	1	HH84
1313	BCD	17.15	0.45	A	1254	7.84	-0.20	2	HH87
1326	Sa	13.41	1.89	A	497	< 7.24	1.52	-	M94
1330	Sa	13.17	1.96	S	1777	7.94	0.85	2	HG86
1356	Sm/BCD	15.55	1.10	A	1251	8.34	0.04	1	HG86
1358	Sa	16.00	0.89	A	-	< 7.31	0.92	-	T.W.
1374	Im/BCD	15.33	1.20	A	2555	8.23	0.23	2	HG86
1375	Sc	12.00	4.76	S	1732	9.56	-0.05	1	HH84
1377	Im	16.87	0.61	A	-	< 6.65	1.25	-	T.W.
1379	Sc	12.62	2.85	A	1505	8.95	0.15	1	HH84
1393	Sc	14.01	1.69	A	2100	8.43	0.23	1	HG86
1401	Sbc	10.27	7.23	A	2284	9.36	0.55	1	HH84
1403	Im	17.15	0.71	A	-	< 7.02	1.00	-	HH87
1410	Sm	14.57	1.48	A	1629	8.20	0.42	1	HH87
1411	Pec	15.72	0.70	A	911	7.96	0.51	3	HH87
1412	Sa	12.12	4.33	A	1342	< 7.02	2.33	-	M94
1426	Im	15.64	0.80	A	1110	< 6.78	1.34	-	HH87
1427	Im/BCD	15.68	0.85	A	-132	7.90	0.27	3	HH87
1435	Im	14.63	1.16	S	609	< 6.58	1.84	-	T.W.
1437	BCD	15.12	0.59	S	1148	8.23	-0.36	2	HB03
1442	Sd	14.82	2.92	S	1735	8.81	0.37	1	HL89

Table 2: Continue

VCC	Type	m_p (mag)	a (arcmin)	Cloud	V km s ⁻¹	$\log M_{HI}$ (M_\odot)	Def_{HI}	Qual	Ref.
1450	Sc	13.29	2.60	A	-173	8.47	0.54	1	SS90
1455	Im	16.80	0.64	S	1339	7.16	0.79	4	HH87
1459	BCD	16.30	0.73	S	1774	7.28	0.77	4	HH87
1465	Im	15.00	1.10	S	734	7.54	0.84	3	HH87
1468	Im	15.00	1.00	S	1233	8.32	-0.01	2	HH87
1507	Sm	15.08	1.16	S	910	8.21	0.22	2	HH87
1508	Sc	12.34	3.60	S	1212	9.54	-0.26	1	HH84
1516	Sbc	12.73	4.04	S	2330	8.68	0.80	1	HH84
1524	Sd	13.51	3.20	A	262	9.25	0.01	1	HL89
1529	Sdm	14.63	1.16	S	1138	8.02	0.40	3	HH87
1532	Sc	14.05	1.87	A	2335	7.93	0.82	2	HG86
1540	Sb	11.32	5.86	S	1736	9.84	-0.13	1	HW89
1552	Sa	12.58	4.24	A	195	< 7.16	2.18	-	M94
1554	Sm	12.30	2.60	S	2021	9.46	-0.37	1	HH84
1555	Sc	10.51	8.33	S	1962	9.79	0.19	1	HH84
1557	Scd	14.53	2.60	S	1759	8.65	0.44	1	HL89
1562	Sc	11.01	7.23	S	1807	9.71	0.15	1	P79
1566	Sd	14.80	1.16	S	427	8.02	0.40	2	HG86
1569	Scd	15.00	1.07	A	799	7.47	0.90	2	HG86
1572	BCD	16.00	0.93	S	1848	8.05	0.19	2	HH87
1575	Sm	13.98	2.00	S	597	7.94	0.93	2	HL89
1581	Sm	14.55	1.46	S	2065	8.64	-0.03	2	HH87
1585	Im	15.45	1.67	A	666	8.79	-0.07	1	HH87
1588	Scd	12.81	2.60	A	1288	8.40	0.68	1	SS90
1596	Im	17.24	0.35	S	1286	7.34	0.12	4	HH87
1597	Sc	15.20	0.93	S	841	7.54	0.63	1	T.W.
1605	Sd	17.00	1.00	A	1077	7.74	0.56	2	HL89
1615	Sb	10.98	6.00	A	484	8.93	0.80	1	W86
1624	Sc	13.89	2.48	S	1151	8.34	0.64	1	HW89
1644	Sm	17.50	0.98	A	756	8.15	0.14	1	HH87
1654	Im	15.96	0.85	A	2051	8.13	0.04	2	HH87
1673	Sc	12.08	2.92	A	2277	8.69	0.43	3	HS82
1675	Pec	14.47	1.26	S	1795	7.45	1.35	3	HH87
1676	Sc	11.70	5.10	A	2255	8.99	0.58	3	HS82
1678	Sd	13.70	2.16	S	1073	9.00	-0.06	2	HL89
1685	Sd	15.18	2.16	S	1443	8.61	0.32	1	HL89
1686	Sm	13.95	2.79	A	1122	8.35	0.79	1	HH87
1690	Sab	10.25	10.73	A	-216	8.93	1.07	1	HR89
1696	Sc	11.81	4.58	A	342	8.94	0.54	1	HH84
1699	Sm	14.11	1.55	S	1635	8.62	0.04	2	HH87
1725	Sm/BCD	14.51	1.55	S	1068	8.11	0.55	2	HH87
1726	Sdm	14.54	1.29	S	61	8.52	0.00	2	HH87
1727	Sab	10.56	6.29	A	1520	8.79	0.83	1	HS81
1728	Im	16.63	0.50	E	-117	7.35	0.38	5	HH87
1730	Sc	12.61	2.16	S	1032	7.83	1.03	3	HH84
1744	BCD	17.50	0.51	E	1150	7.16	0.60	2	HW89
1750	BCD	16.50	0.31	S	-117	7.35	-0.01	4	HH87
1753	Im	16.81	0.71	A	737	7.70	0.32	4	HH87
1757	Sa	13.60	1.87	A	1783	7.38	1.38	5	HG86
1758	Sc	14.99	1.71	S	1788	8.28	0.39	1	HL89
1760	Sa	12.54	4.33	S	792	8.20	1.16	1	HH84
1771	Im	17.97	0.31	E	-	< 7.02	0.34	-	HW89
1780	Sb	13.70	1.87	S	2424	8.41	0.48	1	HL89
1784	Im	15.84	0.79	E	57	7.34	0.78	4	HH87
1789	Im	15.07	1.10	S	1619	7.86	0.53	1	HH87
1791	Sm/BCD	14.67	1.29	S	2079	8.63	-0.12	2	HH87
1804	Im/BCD	15.63	0.75	E	1898	7.23	0.84	5	HH87
1811	Sc	12.92	2.16	E	632	8.63	0.23	1	HH84
1813	Sa	11.51	4.76	E	1834	< 7.19	2.23	-	M94
1816	Im	16.20	1.16	E	1002	8.31	0.12	2	HH87
1822	Im	15.60	0.63	S	1012	7.64	0.29	2	HH87
1859	Sa	12.52	5.10	E	1645	7.81	1.66	2	M94
1868	Scd	13.75	3.95	E	2255	8.53	0.89	1	HG86
1885	Im	16.41	1.16	E	-	< 6.52	1.90	-	T.W.
1918	Im	15.80	1.03	S	980	8.16	0.17	2	HH87
1923	Sbc	13.14	2.31	S	742	8.62	0.45	1	HL89
1929	Scd	13.77	2.48	E	291	8.70	0.35	1	SS90
1931	Im	15.20	1.26	E	1100	8.40	0.10	3	HH87
1932	Sc	13.19	2.92	E	116	8.66	0.45	1	M94
1933	Sm	15.80	0.71	S	2409	8.02	0.00	2	HL89
1943	Sb	12.19	3.20	E	1048	9.03	0.25	1	HS81
1952	Im	16.00	0.71	E	1308	8.21	-0.19	2	HH87
1955	S/BCD	14.32	1.36	E	2012	7.72	0.83	3	HH87
1960	Im/BCD	17.00	0.46	E	-	< 7.09	0.58	-	HH87
1965	Im	16.50	0.50	S	954	7.30	0.44	4	HH87
1970	Im	15.80	0.71	E	1324	6.95	1.07	3	T.W.
1972	Sc	12.03	2.60	E	1422	8.75	0.27	1	HH84
1987	Sc	11.14	4.99	E	1039	9.85	-0.29	1	HS81
1992	Im	15.50	0.81	E	1003	8.35	-0.22	1	HH87
1999	Sa	13.08	1.99	E	510	< 7.19	1.61	-	M94
2007	Im/BCD	15.20	0.78	E	1857	7.37	0.74	3	HH87

Table 2: Continue

VCC	Type	m_p (mag)	a (arcmin)	Cloud	V km s ⁻¹	$\log M_{HI}$ (M_\odot)	Def_{HI}	Qual	Ref.
2015	BCD	16.20	0.51	E	2545	< 7.09	0.67	-	HH87
2023	Sc	13.86	2.01	E	958	8.85	-0.05	1	HG86
2033	BCD	14.65	0.73	E	1486	7.45	0.61	3	HH87
2034	Im	15.82	0.78	E	1500	7.83	0.27	3	HH87
2037	Im/BCD	15.92	0.88	E	1142	7.39	0.81	3	HH87
2058	Sc	11.55	5.86	E	1620	8.79	0.90	1	HH84
2070	Sa	11.53	5.67	E	1008	9.54	0.01	1	HH84
2089	BCD	17.50	0.39	E	-	< 7.09	0.46	-	HH87
2094	Im	17.80	0.37	E	-	< 6.54	0.95	-	HW89

Column 1: VCC designation.

Column 2: Morphological type from Binggeli et al. (1985; 1993);

Column 3: Apparent photographic magnitude from Binggeli et al. (1985);

Column 4: Optical major diameter, in arcmin;

Column 5: Subcloud membership as in Gavazzi et al. (1999b);

Column 6: Recessional velocity, in km s⁻¹;

Column 7: H_I mass or mass limit in solar units;

Column 8: H_I deficiency parameter as defined in Haynes & Giovanelli (1984);

Column 9: Quality flag (see last Column of Table 1).

Column 10: Reference to the H_I measurement;

7. Appendix A: Notes on individual galaxies

VCC 48: The possible line emission of this object, which has an optical redshift of -52 ± 60 km s⁻¹, is masked by Galactic H_I emission. The object remains undetected in spite of the noise reduction from 1.1 mJy, as reported by Hoffman et al. (1987), to 0.64 mJy rms in the present work.

VCC 222: We did not detect this galaxy, with an rms noise level of 0.60 mJy. Its optical redshift, 2298 ± 122 km s⁻¹, is not well determined. An Effelsberg H_I detection was reported by Huchtmeier (1982) at 2410 km s⁻¹, with $W_{50}=273$ km s⁻¹ and $I_{HI}=4.4 \pm 1.5$ Jy km s⁻¹, with an average line signal of 16 mJy. Although Magri (1994) reported a tentative detection at 2596 km s⁻¹, its low signal-to-noise ratio makes it appear spurious. Two published (Krumm & Salpeter 1979; Mirabel & Wilson 1984) estimated upper limits to its line flux are 2.4 and 3.4 Jy km s⁻¹, respectively. We conclude that the line signal reported by Huchtmeier is spurious and due to RFI.

VCC 227, 256: Marginal detections.

VCC 323: The object remains undetected in spite of the noise reduction from 6.0 mJy, as reported by Huchtmeier & Richter (1986), to 0.53 mJy rms in the present work.

VCC 341: We did not detect this galaxy, with an rms noise level of 0.76 mJy. Its optical redshift is 1827 ± 60 km s⁻¹. The Effelsberg H_I detection reported by Huchtmeier (1982) at 1846 km s⁻¹, with $W_{50}=465$ km s⁻¹ and $I_{HI}=3.0 \pm 1.5$ Jy km s⁻¹, i.e. an average line strength of 6.5 mJy, appears spurious given its low signal-to-noise ratio.

VCC 358: Bad baselines due to the proximity of the 19 Jy continuum source NGC 4261 resulted in the very high rms noise level of 28 mJy, about 30 times that of similar observations made for this project. Our previous Nançay observations (van Driel et al. 2000) also had a high rms noise level of 11 mJy and a limit of 6 Jy km s⁻¹ was reported by Huchtmeier & Richter (1986) from Effelsberg data. An Arecibo detection at 2633 km s⁻¹ with $I_{HI}=9.0$ Jy km s⁻¹ was reported by Magri (1994).

VCC 362: Given that its optical redshift is 156 ± 44 km s⁻¹, our H_I detection ($V_{HI}=2350$ km s⁻¹, $W_{50}=92$ km s⁻¹ and $I_{HI}=0.40$ Jy km s⁻¹) must be due to confusion. At 4' lies VCC 367, a 17.4 mag object without published optical redshift, for which Hoffman et al. (1987) measured $V_{HI}=2362$ km s⁻¹, $W_{50}=98$ km s⁻¹ and $I_{HI}=0.59$ Jy km s⁻¹ at Arecibo. VCC 362 remains undetected in spite of the noise reduction from 3.5 mJy, as reported by Magri (1994), to 0.44 mJy rms in the present work.

VCC 524: Besides a detection of the target galaxy at 1035 km s⁻¹, our spectrum shows a detection near 5800 km s⁻¹ with $I_{HI}=0.45$ Jy km s⁻¹, which is due to confusion by VCC 526 (= NGC 4307A), a 15.7 mag Sc spiral 3'2 away, with $V_{opt}=5989 \pm 46$ km s⁻¹, for which Magri (1994) measured $V_{HI}=5836$ km s⁻¹, $W_{50}=76$ km s⁻¹ and $I_{HI}=2.6$ Jy km s⁻¹ at Arecibo.

VCC 528: is a background galaxy, at 7046 Jy km s⁻¹.

VCC 666: The possible detection at -250 km s⁻¹ is doubtful. The object remains undetected in spite of the noise reduction from 1.3 mJy, as reported by Hoffman et al. (1987), to 0.51 mJy rms in the present work.

VCC 802: The object remains undetected in spite of the noise reduction from 1.5 mJy, as reported by Hoffman et al. (1987), to 0.58 mJy rms in the present work.

VCC 1086: its optical redshift is 294 ± 39 km s⁻¹. Our H_I parameters ($V_{HI}=328 \pm 8$ km s⁻¹, $W_{50}=240$ km s⁻¹ and $I_{HI}=0.93 \pm 0.09$ Jy km s⁻¹) are comparable to those ($V_{HI}=363$ km s⁻¹, $W_{50}=224$ km s⁻¹ and $I_{HI}=0.96$ Jy km s⁻¹) measured by Hoffman et al. (1989a) at Arecibo. Profile contaminated by galactic absorption.

VCC 1189: its optical redshift is 544 ± 43 km s⁻¹. Our H_I profile has $V_{HI}=516 \pm 1$ km s⁻¹, $W_{50}=112$ km s⁻¹ and

$I_{HI}=4.2\pm0.1$ Jy km s $^{-1}$. The profile parameters measured by, respectively, Huchtmeier & Richter (1986) at Effelsberg, Hoffman et al. (1989a) at Arecibo and Schneider et al. (1992) with the NRAO 300ft are $V_{HI}=530$, 537 and 543 km s $^{-1}$, $W_{50}=98$, 110 and 121 km s $^{-1}$ and $I_{HI}=5.0$, 3.6 and 9.7 Jy km s $^{-1}$. Although the line fluxes vary considerably, they do not correlate with the size of the telescope beam, nor are there any candidates for confusion in the vicinity. The large line flux measured by Schneider et al. appears to be spurious.

VCC 1196: We did not detect this galaxy, with an rms noise level of 0.57 mJy. Its optical redshift is 908 ± 36 km s $^{-1}$. An Effelsberg H I detection was reported by Huchtmeier & Richter (1986) at 2422 km s $^{-1}$, with $W_{50}=446$ km s $^{-1}$ and $I_{HI}=6.5\pm1.5$ Jy km s $^{-1}$, i.e. an average line strength of 15 mJy, which we assume is spurious and due to RFI.

VCC 1287: The object remains undetected in spite of the noise reduction from 1.4 mJy, as reported by Hoffman et al. (1987), to 0.77 mJy rms in the present work.

VCC 1377: The object remains undetected in spite of the noise reduction from 1.1 mJy, as reported by Hoffman et al. (1987), to 0.51 mJy rms in the present work.

VCC 1435: The object remains undetected in spite of the noise reduction from 0.9 mJy, as reported by Hoffman et al. (1987), to 0.44 mJy rms in the present work.

VCC 1448: We did not detect this galaxy, which does not have a published optical redshift, with an rms noise level of 0.92 mJy. An Effelsberg H I detection was reported by Huchtmeier & Richter (1986) at 2583 km s $^{-1}$, with $W_{50}=66$ km s $^{-1}$ and $I_{HI}=1.5\pm0.26$ Jy km s $^{-1}$, i.e. with an average line signal of 23 mJy, which we assume is spurious and due to RFI.

VCC 1885: The object remains undetected in spite of the noise reduction from 0.7 mJy, as reported by Hoffman et al. (1987), to 0.38 mJy rms in the present work.

VCC 1970: Hoffman et al. (1987) reported undetection with 1.0 mJy rms. We detected it at a noise level of 0.37 mJy rms.